CASPT2 Study of Inverse Sandwich-Type Dinuclear 3d Transition Metal Complexes of Ethylene and Dinitrogen Molecules: Similarities and Differences in Geometry, Electronic Structure, and Spin Multiplicity

Masayuki Nakagaki and Shigeyoshi Sakaki*

Fukui Institute for Fundamental Chemistry, Kyoto University, Takano-Nishihiraki-cho, Sakyo-ku, Kyoto 606-8103, Japan

Abstract

Spin multiplicities and coordination structures of inverse sandwich-type complexes (ISTCs) of ethylene and dinitrogen molecules with 3d transition metal elements (Sc to Ni), $(\mu\text{-}C_2H_4)[M(AIP)]_2$ and $(\mu\text{-}N_2)[M(AIP)]_2$ (AIPH = (Z)-1-amino-3-imino-prop-1-ene; M = Sc to Ni), were investigated with the CASPT2 method. In both of the ethylene and dinitrogen ISTCs of the early 3d transition metals (Sc to Cr), sandwiched ethylene and dinitrogen ligands coordinate with two metal atoms in an η^2-side-on mode and their ground states take an open-shell singlet spin multiplicity. The η^1-end-on coordination structure of dinitrogen ISTCs is much less stable than the η^2-side-on one in these metals. For the late 3d transition metals (Mn to Ni), ethylene and dinitrogen ISTCs exhibit interesting similarities and differences in spin multiplicity and structure, as follows: In the ethylene ISTCs of Mn to Ni, the ground state takes an open-shell singlet spin multiplicity like those of the ISTCs of early transition metals. However, the ethylene ligand is considerably distorted, in which the ethylene carbon atoms have a tetrahedral-like structure similar to an sp^3-carbon and each of them coordinates with one metal in a $\mu\text{-}\eta^1\text{:}\eta^1$-structure. These geometrical features are completely different from those of ISTCs of the early transition metals. In the dinitrogen ISTCs of Mn to Ni, on the other hand, the ground state takes a high spin multiplicity from nonet (Mn) to triplet (Ni). The η^2-side-on coordination structure of the dinitrogen ligand is as stable as the η^1-end-on one in the Mn complex but the η^1-end-on structure is more stable than the η^2-side-on one in the Fe to Ni complexes. All these interesting similarities and differences between ethylene and dinitrogen ISTCs and between the early and late transition metal elements arise from occupations of several important molecular orbitals.

1. Introduction

Spin multiplicity of transition metal complex is attracting a lot of interests recently because the spin multiplicity deeply relates to a single-molecule magnet,[1-3] spin-cross-over complex,[4-6] spin-catalysis,[7-10] and so on. In this regard, it is of considerable interest to obtain theoretical knowledge of how to understand spin multiplicity and how to control it. In general, it is said that the strong ligand field leads to the presence of low spin state and the weak ligand field leads to the presence of high spin state. However, the story is not so simple in dinuclear transition metal complex, because of the presence of the interaction between two metal centers.

Recently, inverse sandwich-type dinuclear transition metal complexes (ISTCs) were synthesized.[11-25] In the ISTCs, an organic moiety is sandwiched by two metal moieties in contrast to the usual sandwich-type complex in which a metal is sandwiched by two organic moieties; for instance, see ferrocene and chromocene. The ISTCs draw great interests in coordination chemistry, organometallic chemistry, and physical chemistry because of their characteristic geometries, bonding natures, and molecular properties. For instance, the benzene[15] and toluene[16,17] ISTCs of Cr have a septet ground state and those of V(I) have a quintet ground state, which are unusually high spin multiplicities. Theoretical studies clearly elucidated the reason why such high spin multiplicity is possible in these complexes.[26,27] However, the ISTC of Cr(I) does not always have a high spin multiplicity. For instance, the dinitrogen ISTC of Cr, $(\mu\text{-}\eta^2\text{:}\eta^2\text{-}N_2)[Cr(DDP)]_2$ (DDPH = 2-{(2,6-diisopropylphenyl)amino}-4- {(2,6-diisopropylphenyl)imino}pent-2-ene), exhibits an effective magnetic moment of 3.9 μ_B, which corresponds to the spin multiplicity between triplet and quartet.[14] According to the recent CASPT2 calculation, this complex has an open-shell singlet ground state[28] in contrast to the benzene ISTC of Cr which has a septet ground state and the effective magnetic moment is a thermal average of singlet to nonet states. In the dinitrogen ISTC

of Fe, $(\mu\text{-}\eta^1\text{:}\eta^1\text{-}N_2)[Fe(DDP)]_2$, on the other hand, the ground state with a septet spin multiplicity was experimentally reported[13] and also theoretically calculated.[28] Interestingly, this high spin multiplicity is very different from the theoretically calculated open-shell singlet ground state of the benzene ISTC of Fe.[26] These results suggest that the spin multiplicity of ISTC is flexible and the molecule sandwiched by two metal moieties as well as the metal center plays crucial roles in determining the spin multiplicity. The theoretical knowledge of the factors for determining spin multiplicity is crucial for well understanding the spin state and synthesizing a new compound with various spin states.

The ethylene ISTC of Cr(I) was also experimentally reported.[14] Its magnetic moment is 4.2 μ_B, similar to the dinitrogen ISTC of Cr. This similarity is not surprising, because both of ethylene and dinitrogen molecules coordinate with the Cr atoms in an η^2-side-on mode. However, some differences are expected to be found between the dinitrogen and ethylene ISTCs of Fe(I) because dinitrogen molecule coordinates with the Fe centers in an η^1-end-on mode[13] but ethylene is unable to take an end-on coordination structure because of the presence of hydrogen atoms.

In our previous study of the benzene ISTCs,[26] we found that the spin multiplicity of the ground state monotonously increases from a closed-shell singlet to a nonet when going from Sc to Mn but suddenly decreases to an open-shell singlet in Fe. Hence, it is of considerable interest to systematically investigate the spin multiplicity of the ethylene and dinitrogen ISTCs of all first-row transition metal elements and elucidate how the spin multiplicity changes along the first-row transition metal elements. In this work, we theoretically investigated the ethylene and dinitrogen ISTCs of Sc to Ni. Our main purposes are to clarify the similarities and differences in geometry, electronic structure, spin multiplicity, and spin distribution between ethylene and dinitrogen ISTCs and between early transition metal elements (Sc to Cr) and late ones (Mn to Ni), elucidate the

reasons of similarities and differences, and disclose the important factors for determining a spin multiplicity.

2. Computational Details

We employed a model ligand AIP (AIPH = 1-amino-3-imino-prop-1-ene) instead of the real DDP ligand to save the computational cost; see Figure 1. This model was successfully employed in our previous studies.[26-28] Geometry optimization was carried out at each spin state by the complete active space self-consistent field (CASSCF) method.[24] In the geometry optimization, such two kinds of symmetry as D_{2h} and C_{2h} were employed in the ethylene (C_2H_4) complex, the reason of which will be discussed below. In the dinitrogen (N_2) complex, η^1-end-on and η^2-side-on coordination structures were optimized under D_{2h} symmetry.

The z-axis was taken to be along the M-M line and the x-axis was taken to be perpendicular to the M(AIP) plane; see Figure 1. In (μ-N_2)[M(AIP)]$_2$ (M = Sc to Co), the five d orbitals of each metal and the π^* orbitals of the dinitrogen molecule were employed in an active space. The number of total active orbitals is 12. To examine whether or not the inclusion of π orbitals of the dinitrogen molecule influences the computational results, we carried out CASPT2 calculations of (μ-N_2)[Co(AIP)]$_2$ employing a larger active space which consists of 14 active orbitals including two π orbitals of the dinitrogen molecule. The relative energies of the η^2-side-on and η^1-end-on structures are changed little by the inclusion of π orbitals; see Table S1 and the discussion in supporting information (SI) for details. This result indicates that the inclusion of π orbitals is not important in discussing (μ-N_2)[M(AIP)]$_2$ (M = Sc to Co). In the case of the Ni analogue (μ-N_2)[Ni(AIP)]$_2$, on the other hand, we employed a larger active space including the π orbitals because the relative stabilities of spin states are somehow influenced by the inclusion of π orbitals; see Table S1 in the supporting information. In (μ-C_2H_4)[M(AIP)]$_2$, however, the π orbital

could not be involved in the active space even in the Ni complex because the π orbital went out from the active space during CASSCF calculation. This means that the π orbital is not important in the active space of (μ-C_2H_4)[Ni(AIP)]$_2$. Hence, we employed the active space consisting of 11 orbitals in all these ethylene complexes.

The second-order perturbation (PT2) calculation was carried out with a CASSCF-optimized structure, using a CASSCF wavefunction as a reference.[29-31] The energy denominator shift (EDS) technique[32] was employed in the PT2 calculation, where the EDS value of 0.2 a.u. was used throughout the present study. The CASSCF calculation with spin-orbit coupling interaction was carried out but the relative energy of each spin state is influenced little by the spin-orbit coupling; see Table S2 in SI.

Edmiston-Ruedenberg localization[33] was applied to CASSCF active orbitals and then CASCI calculation was carried out with these localized orbitals to evaluate the occupation number and the spin density of each localized orbitals. The electron and spin populations of the M(AIP) moiety and such a sandwiched molecule as ethylene and dinitrogen were evaluated with the CASCI wavefunction.

For metal atoms, (311111/22111/411/1) basis sets were employed with the effective core potentials of the Stuttgart-Dresden-Bonn group.[34] For C, N, and H atoms, cc-pVDZ basis sets were employed.[35] One augmented function was added to each N atom in AIP and dinitrogen and each C atom in ethylene, considering that AIP is anionic and the electron population considerably increases in ethylene and dinitrogen moieties through the back-donation interaction.

The CASSCF and the CASPT2 calculations were carried out by GAMESS[36] and MOLCAS 6.4,[37] respectively.

3. Results and Discussion

3.1. Geometries and spin multiplicities of ethylene and dinitrogen ISTCs.

3.1.1. Comparisons of calculated-geometry and spin multiplicity of an ethylene ISTC of Cr, (μ-C_2H_4)[Cr(AIP)]$_2$, with their experimental values. Because (μ-C_2H_4)[Cr(DDP)]$_2$ has been experimentally reported[14] and its dinitrogen analogue (μ-N_2)[Cr(DDP)]$_2$ has been discussed in our previous work,[28] we wish to firstly focus on the ethylene ISTC of Cr. Important geometrical parameters optimized in an open-shell singlet state by the CASSCF method are shown in Figure 2, because the ground state has an open-shell singlet spin multiplicity, as will be discussed below. The D_{2h}-optimized structures at singlet to nonet spin states resemble each other; see Table S3 in SI for geometrical parameters of other spin states. Both the Cr-Cr distance and the C-C bond length of the ethylene moiety are close to the experimental values.[14] The geometry optimization was also carried out under C_{2h} symmetry because the experimentally reported Cr-C distances are moderately different from each other.[14] In the C_{2h} structure, the ethylene moiety considerably distorts and the geometrical parameters become considerably different from the experimental values. Hence, we wish to first discuss what spin multiplicity the ground state has and which of D_{2h} and C_{2h} symmetries is an equilibrium geometry.

As listed in Table 1, the ground state has an open-shell singlet spin multiplicity in both of D_{2h} and C_{2h} geometries and the energy difference among the singlet to the nonet states is small at the CASPT2 level like the dinitrogen ISTC of Cr investigated previousry.[28] It should be noted that the D_{2h} structure is somewhat more stable than the C_{2h} one at all these spin multiplicities at the CASPT2 level except for the nonet spin state; see Table 1.[38] Because the singlet to nonet states are close in energy, the experimentally observed magnetic moment corresponds to the thermal average of these spin multiplicities like it in the dinitrogen ISTC of Cr.[28] According to the Boltzmann distribution law, the average of effective magnetic moments was estimated to be μ_{eff} = 4.0 and 1.6 μ_B with the CASSCF and CASPT2-calculated energies, respectively, at 293 K.

Though the CASSCF-calculated value is close to the experimental value, the CASPT2-calculated value is somewhat smaller than the experimental one (4.2 μ_B); several factors must be examined in furture.[39] Based on these results, it is concluded that the ethylene ISTC of Cr(I) has a D_{2h} structure with an open-shell singlet ground state, while the energy and the geometry are similar among the singlet to the nonet.

3.1.2. Comparisons of geometry and spin multiplicity of ethylene and dinitrogen ISTCs, (μ-C_2H_4)[M(AIP)]$_2$ and (μ-N_2)[M(AIP)]$_2$, among M = Sc to Ni. Interestingly, the geometry completely changes when going from the ethylene ISTC of Cr to a Mn analogue. In the Mn analogue, the D_{2h} structure is much more unstable than the C_{2h} one, as shown in Table 1. In the C_{2h} structure, the distances between the Mn and the ethylene carbon atoms are 2.18 and 3.12 Å, indicating that the ethylene coordinates with two Mn atoms in a μ-η^1:η^1-structure. This coordination structure is similar to that of the benzene ISTC of Ni(I) in which three carbon atoms of benzene coordinate with one Ni atom and the other three carbon atoms coordinate with the other Ni atom.[19] And also in the benzene ISTC of Nb, four carbon atoms coordinate with one Nb atom the other two coordinate with another Nb atom.[25] Despite of the difference in geometry, the ground state has a singlet spin multiplicity and the energy difference among the singlet to the undectet spin states is small like in the above-discussed Cr analogue. These results suggest that interesting similarities and differences are found between the early (Sc to Cr) and late (Mn to Ni) transition metal complexes, which will be discussed below in more detail.

As shown in Table 1, we investigated both C_{2h} and D_{2h} geometries in the other ethylene ISTCs (μ-C_2H_4)[M(AIP)]$_2$ because (μ-C_2H_4)[Cr(AIP)]$_2$ has a D_{2h} geometry but the Mn analogue has a C_{2h} one. The Sc to V complexes have a D_{2h} structure like the Cr complex, whereas the Fe to Ni complexes have a C_{2h} structure like the Mn complex.

Interestingly, the ground states of all these complexes have an open-shell singlet spin multiplicity despite of the different geometry. It is noted that the highest spin multiplicity whose energy is close to that of the ground state increases from triplet to undectet when going from Sc to Mn and then decreases from undectet to quintet when going from Mn to Ni. This is completely different from the benzene ISTCs of the first-row transition metal elements, in which the spin multiplicity of ground state increases from closed-shell singlet to nonet when going from Sc to Mn and then decreases to open-shell singlet when going to Fe.[26] Also, it should be noted that the energy difference between these spin multiplicities is very small in these ethylene ISTCs like the dinitrogen ISTC of Cr;[28] see Table 1. This is different from the benzene ISTC in which the energy difference between spin multiplicities is considerably large.[26]

In the dinitrogen ISTCs, $(\mu\text{-}N_2)[M(AIP)]_2$ (M = Sc to Ni), we investigated relative energies of various spin states in both of η^1-end-on and η^2-side-on coordination structures, as listed in Table 2. In the dinitrogen ISTCs of Sc to Cr (the early transition metal elements), the η^2-side-on coordination structure is considerably more stable than the η^1-end-on one. The ground state takes an open-shell singlet spin multiplicity and the energy difference between the singlet and other spin states is very small in these Sc to Cr complexes. When going from Sc to Cr, the highest spin multiplicity whose energy is close to that of the singlet increases from triplet to nonet like that of the ethylene ISTCs of Sc to Cr. These similarities between ethylene and dinitrogen ISTCs are listed in Table S5 in SI.

In the dinitrogen ISTC of Mn, the stabilities of the η^1-end-on and the η^2-side-on structures are comparable. In the dinitrogen ISTCs of Fe to Ni, the η^1-end-on structure is somewhat more stable than the η^2-side-on one. The ground state has a high spin multiplicity and the energy difference between spin states is large in these Mn to Ni complexes, as compared in Table 2. The spin multiplicity of the ground state decreases

from nonet to triplet when going from Mn to Ni. It should be noted that the coordination structure of dinitrogen molecule and spin multiplicity are different between the dinitrogen ISTCs of Sc to Cr and those of Mn to Ni and that the spin multiplicity is completely different between the dinitrogen and ethylene ISTCs of Mn to Ni. The similarities and differences between the ethylene and dinitrogen ISTCs and between early and late transition metal elements are summarized in Table S5. The next work is to elucidate the reasons of these similarities and differences, which will be discussed below.

3.2. Electronic structures and MO diagrams of ethylene and dinitrogen ISTCs.

3.2.1. MO diagram and orbital occupation of ethylene ISTCs, (μ-C_2H_4)[M(AIP)]$_2$ (M = Sc to Ni). It is of considerable interest to investigate the reason why the spin multiplicities of these ethylene ISTCs are different from those of the benzene ISTCs. The CASSCF(10,11)-calculated natural orbitals in the ^1A_g state of (μ-η^2:η^2-C_2H_4)[Cr(AIP)]$_2$ are shown in Figure 3(A). The most stable ψ_1 MO contains a bonding overlap between the Cr d_{yz} and the π* orbital of ethylene. It is doubly occupied in a formal sense. The occupation numbers of the other ψ_2 to ψ_9 MOs are close to 1.0.

This electronic structure is understood by the orbital interaction diagram shown in Figure 3(A). The most stable $\psi_{1,b2g}$ MO mainly consists of a bonding overlap between the π* orbital of ethylene and the d_{yz} orbital of metal. Its anti-bonding counterpart is the most unstable $\psi_{11,b2g}$ MO; See Figure S2 and discussion in SI for details. The other $\psi_{2,b1u}$ to $\psi_{9,b2u}$ MOs are nearly non-bonding and thereby nearly degenerate. Because the Cr(I) has five d electrons, totally ten d electrons occupy these MOs. Hence, the most stable $\psi_{1,b2g}$ is doubly occupied and the $\psi_{2,b1u}$ to $\psi_{9,b2u}$ are singly occupied; see Figure 3(A). It should be noted that the $\psi_{10,b3u}$ mainly consisting of the Cr d_{yz} orbital is empty. In such electronic state, one-electron excitation from the $\psi_{1,b2g}$ to the unoccupied $\psi_{11,b2g}$ MO does not induce the exchange interaction with the $\psi_{10,b3u}$. This means that a high spin state is

not stabilized well by spin polarization. This explanation will be discussed in more detail by a model calculation below; see section 3.4.3. In the benzene ISTC of Cr, on the other hand, non-bonding d MOs are singly occupied, which is favorable for a high spin state because the spin polarization can be induced by these MOs; see page S9 (Figure S3) in the supporting information.

Because the ground state has an open-shell singlet spin multiplicity, four electrons of the $\psi_{2,b1u}$ to $\psi_{9,b2u}$ have an α-spin and the other four electrons have a β-spin. In such case, the energy differences between two spin states are very small because these eight electrons afford singlet, triplet, quintet, septet, and nonet spin states through various combinations, as has been shown in Table 1. Though both of the $\psi_{6,b1u}$ and $\psi_{7,ag}$ mainly consist of the metal d_{z2} orbital and both of the $\psi_{8,b3g}$ and $\psi_{9,b2u}$ mainly consist of the metal d_{xz} orbital, the occupation numbers of the $\psi_{6,b1u}$ and $\psi_{8,b3g}$ are moderately larger than those of the $\psi_{7,ag}$ and $\psi_{9,b2u}$, respectively, as shown in Figure 3(A) and Table 3. In the $\psi_{7,ag}$, the two d_{z2} orbitals overlap with the doubly occupied C-C σ-bonding orbital of ethylene in an anti-bonding way, because the σ-orbital exists at a lower energy than the Cr d orbital; see Figures S4(A) and S4(B) for the detailed figures of $\psi_{6,b1u}$ to $\psi_{9,b2u}$.[40] Also, the $\psi_{9,b2u}$ is anti-bonding between the d orbital of Cr(AIP) and the doubly occupied C-H σ-orbitals of ethylene. The $\psi_{6,b1u}$ and $\psi_{8,b3g}$ are, on the other hand, completely non-bonding between Cr(AIP) and ethylene which does not have any anti-bonding overlap at all between the Cr and ethylene.

In the open-shell singlet state, the larger occupations of the $\psi_{6,b1u}$ and $\psi_{8,b3g}$ than those of the $\psi_{7,ag}$ and $\psi_{9,b2u}$ are possible, while the occupation numbers of all these orbitals are 1.0 in the high spin state. As well known, the high spin state is favorable for stabilizing the compound by exchange interaction but unfavorable for the stabilizing the compound by orbital occupation. It is likely concluded that the open-shell singlet ground state of this ethylene ISTC of Cr receives the stabilization energy by larger occupations in the $\psi_{6,b1u}$

and $\psi_{8,b3g}$ than in the $\psi_{7,ag}$ and $\psi_{9,b2u}$.

The occupation numbers of CASSCF natural orbitals of (μ-C_2H_4)[M(AIP)]$_2$ (M = Sc to Ni) in the ground state are shown in Table 3. The ethylene ISTCs of Sc to V have an open-shell singlet ground state, too, as shown in Table 1. In the V complex, eight d electrons occupy these MOs. The most stable $\psi_{1,b2g}$ is doubly occupied. Though the $\psi_{2,b1u}$ to $\psi_{7,ag}$ are singly occupied in a formal sense, the $\psi_{6,b1u}$ has a moderately larger occupation number than the $\psi_{7,ag}$ like in the Cr complex. The $\psi_{4,au}$ has a larger occupation number than the $\psi_{5,b1g}$, too, because the $\psi_{4,au}$ is completely non-bonding but the $\psi_{5,b1g}$ contains a weakly anti-bonding overlap between the d_{xy} orbital of V and the C-H σ-bonding orbitals of ethylene; see Figure S4(C) in SI.[40]

In the Ti complex, totally six d electrons occupy these MOs; the most stable $\psi_{1,b2g}$ is doubly occupied and the $\psi_{2,b1u}$ to $\psi_{5,b1g}$ are singly occupied, too. The non-bonding $\psi_{2,b1u}$ and $\psi_{4,au}$ have a moderately larger occupation number than the $\psi_{3,ag}$ and $\psi_{5,b1g}$, respectively.

In the Sc complex, four d electrons occupy these MOs; the most stable $\psi_{1,b2g}$ is doubly occupied, and the remaining two electrons occupy the $\psi_{2,b1u}$ and $\psi_{3,ag}$. The $\psi_{3,ag}$ has a moderately larger occupation number than the $\psi_{2,b1u}$ because the $\psi_{3,ag}$ becomes moderately bonding due to the larger size of 3d orbitals in Sc; see Figure S4(D).[40] Hence, the open-shell singlet is the ground state in these Sc to V complexes.

The ethylene ISTCs of Mn to Ni have a singlet ground state, too, as was shown in Table 1. However, the geometry is very different from those of the Sc to Cr complexes, as discussed above; see also Table S5. It is of considerable interest to elucidate the reason why the spin multiplicity is the same but the geometry is very different from those of the Sc to Cr complexes. In the Mn complex, two more d electrons must be added to these MOs, compared to the Cr complex. In this case, we have to consider two possibilities; in one possibility, the $\psi_{10,bu}$ and $\psi_{11,ag}$ MOs become singly occupied, and in another, the $\psi_{2,bu}$

and $\psi_{3,ag}$ MOs become doubly occupied. The CASSCF calculation indicates that the former electron configuration is the ground state, as shown in Figure 3(B). Also, it is noted that both of the $\psi_{10,bu}$ and $\psi_{11,ag}$ MOs mainly consist of non-bonding d_{yz} orbital of Mn unlike the $\psi_{11,ag}$ MO of the Cr complex which contains an anti-bonding overlap between the Cr d_{yz} and the π^* orbital of ethylene, as will be discussed below in detail. Consistent with these features, the doubly occupied $\psi_{1,ag}$ MO mainly consists of the distorted π^* orbital of ethylene, indicating that the π^* orbital of ethylene is almost doubly occupied. This means that the hybridization of the carbon atoms of ethylene changes from sp^2 to sp^3, which is the origin of the considerably distorted structure of the ethylene ISTC of Mn. In the other $\psi_{2,bu}$ to $\psi_{11,ag}$ MOs, the occupation number is almost 1.0; see Table 3. Actually, the singlet to the undectet spin states are almost degenerate at the CASSCF level (Table S6). However, the ground state becomes an open-shell singlet at the CASPT2 level, because dynamical electron correlation tends to stabilize the low spin state compared to the high spin state.

One important question remains; why does the π^* component of ethylene disappear in the $\psi_{11,ag}$? In the ethylene ISTC of Cr, the $\psi_{10,b3u}$ and $\psi_{11,b2g}$ are unoccupied in a formal sense, while in the Mn analogue they become singly occupied due to the increase in the number of d electrons. Because the $\psi_{11,ag}$ MO of the non-distorted D_{2h} geometry contains the anti-bonding overlap between the Mn d_{yz} and the π^* orbital of ethylene, the occupation of $\psi_{11,ag}$ is unfavorable for stabilizing the compound. If the anti-bonding disappears, the occupation of $\psi_{11,ag}$ is not unfavorable. To decrease the anti-bonding overlap, the geometry distorts to a C_{2h} symmetry and simultaneously the π^* component of ethylene decreases in the $\psi_{11,ag}$. As a result, the d_{yz} component increases in the $\psi_{11,ag}$ and the π^* one increases in the $\psi_{1,ag}$, which increases the electron population in the π^* orbital and thereby induces the hybridization change of the carbon atom from sp^2 toward sp^3; see Figure 3(B).

In the ethylene ISTCs of Fe to Ni, the $\psi_{10,bu}$ and $\psi_{11,ag}$ MOs are singly occupied and some of the singly occupied non-bonding $\psi_{2,bu}$ to $\psi_{9,au}$ MOs become doubly occupied because the number of d electrons further increases. Because the occupation change occurs in non-bonding MOs, the electronic structure of the ethylene moiety changes little from that of the ISTC of Mn. Hence, all these complexes have a distorted ethylene moiety and an open-shell singlet ground state.

3.2.2. MO diagram and orbital occupation of dinitrogen ISTCs, (μ-N_2)[M(AIP)]$_2$ (M = Sc to Ni). The occupation numbers of CASSCF natural orbitals of dinitrogen ISTCs, (μ-N_2)[M(AIP)]$_2$ (M = Sc to Ni) in the ground state are shown in Table 4. These occupation numbers provide well understanding of the difference between the ISTCs of early 3d metal (Sc to Cr) and those of the late 3d one (Mn to Ni).

In the η^2-side-on dinitrogen ISTCs of Sc to Cr, the π_z* orbital of the dinitrogen moiety overlaps well with the metal d_{yz} orbital to form a bonding $\psi_{1,b2g}$ MO and an anti-bonding $\psi_{12,b2g}$ MO, as shown in Figure 4(A). On the other hand, the π_x* MO of dinitrogen, which is perpendicular to the M-M axis, form a weak δ-type overlap with the d_{xy} orbitals to afford the $\psi_{4,b1g}$ and $\psi_{5,au}$ MOs. Hence, the bonding $\psi_{4,b1g}$ and anti-bonding $\psi_{5,au}$ MOs mainly consisting of two d_{xy} orbitals are moderately separated in energy; see Figure 4(A).[40] Because the $\psi_{1,b2g}$ exists at a very low energy, it is doubly occupied in a formal sense, and other $\psi_{2,b1u}$ to $\psi_{9,b2u}$ MOs are singly occupied, as shown in Table 4. These singly occupied MOs are not completely degenerate because of the presence of the π_x, π_x*, and σ-bonding orbitals of dinitrogen, but the energy difference is very small because these MOs contain either the δ-type overlap or smaller one; see Figure S2(B). These MO features of the η^2-side-on dinitrogen ISTCs are essentially the same as those of the ethylene ISTCs in the Sc to Cr. Hence, four to eight d electrons in these MOs provide an open-shell singlet ground state in the dinitrogen ISTCs of Sc to Cr like their ethylene

ISTCs.

As shown in Table 2, the η^1-end-on structure is considerably less stable than the η^2-side-on one in the dinitrogen ISTCs of Sc to Cr. Because totally ten d electrons occupy these MOs in the ISTC of Cr, only the $\psi_{1,b2g}$ MO is doubly occupied unlike the ISTCs of Mn to Ni, which will be discussed below. In the η^1-end-on structure, the metal d_{xz} and d_{yz} orbitals overlap with the π_x^* and π_y^* of dinitrogen to afford two bonding MOs $\psi_{1,b2g}$ and $\psi_{2,b3g}$, respectively. However, these $\psi_{1,b2g}$ and $\psi_{2,b3g}$ MOs are less stable in energy than the $\psi_{1,b2g}$ MO in the η^2-side-on one because the d_π-π^* bonding overlap is smaller in the η^1-end-on structure than in the η^2-side-on one; see Figure S5. Because only one MO is doubly occupied and another is singly occupied in these ISTCs of Sc to Cr, the η^1-end-on structure is less stable than the η^2-side-on.

In the dinitrogen ISTC of Mn, the situation becomes different; because the number of d electrons increases to twelve, two bonding $\psi_{1,b2g}$ and $\psi_{2,b3g(b1g)}$ MOs are doubly occupied in a formal sense in both of the η^1-end-on and η^2-side-on structures,[41] while the $\psi_{3,b1u}$ to $\psi_{10,b3u}$ MOs are singly occupied, as shown in Figures 4(B) and S6. In the η^2-side-on structure, the $\psi_{1,b2g}$ is very stable in energy but the $\psi_{2,b1g}$ is moderately more stable than the other non-bonding MOs, because the $\psi_{1,b2g}$ and $\psi_{2,b1g}$ have d_π-π^* and d_δ-π^* type interactions, respectively. In the η^1-end-on structure, on the other hand, both of the $\psi_{1,b2g}$ and $\psi_{2,b3g}$ are considerably stable because the $\psi_{1,b2g}$ and $\psi_{2,b3g}$ contain the π-type d_π-π^* bonding overlap in this coordination mode; see Figure 4(B). In the η^2-side-on structure, the very stable $\psi_{1,b2g}$ and the moderately stable $\psi_{2,b1g}$ are doubly occupied, while in the η^1-end-on structure, the considerably stable $\psi_{1,b2g}$ and $\psi_{2,b3g}$ are doubly occupied.[41] Thus, the η^1-end-on structure is as stable as the η^2-side-on one in the Mn complex.

In the dinitrogen ISTCs of Fe to Ni, the η^1-end-on structure is somewhat more stable than the η^2-side-on one. Here, we wish to mention that the d-orbital energy becomes lower as going from the left-hand side to the right-hand side in the periodic table. As a

result, the d_π-π^* bonding interaction becomes weaker as going from Mn to Ni. On the other hand, the σ-donation-type charge-transfer (CT) from the lone pair of dinitrogen molecule to the $3d_\sigma$, 4s, and $4p_\sigma$ orbitals becomes larger. Since the lone pair orbital of dinitrogen ligand overlaps with the metal $3d_\sigma$, 4s, and $4p_\sigma$ orbitals to a larger extent than the π orbitals of dinitrogen, the η^1-end-on structure can receive a larger stabilization energy from this σ-donation than the η^2-side-on one. Because of this additional contribution of the σ-donation, the η^1-end-on structure is somewhat more stable than the η^2-side-on one in the Fe to Ni complexes.

3.3. Electron and spin distributions in (μ-N_2)[M(AIP)]$_2$ and (μ-C_2H_4)[M(AIP)]$_2$ (M = Sc to Ni).

We performed CASCI calculation with localized MOs to make a detailed analysis of electron and spin distributions on the N_2 and M(AIP) moieties. The electron populations of the π* orbitals of dinitrogen and ethylene moieties moderately increase when going from Sc to Cr, as shown in Table 5. Then, their electron populations significantly increase in both of ISTCs of ethylene and dinitrogen when going to Mn but change little when going from Mn to Ni. This feature is of considerable interest.

In the ethylene ISTCs of Sc to Cr, the π* orbital is not doubly occupied but becomes doubly occupied in the ISTCs of Mn to Ni, as was discussed above. In the η^2-side-on dinitrogen ISTCs of Sc to Cr, only one π_z^* orbital participates in the π-back donation, which has almost one electron. However, the other π_x^* orbital possesses little electron population because it participates in the δ-type MO; see Table 5. In the dinitrogen ISTCs of Mn to Ni, the $\psi_{1,b2g}$ and $\psi_{2,b3g}$ MOs, which participate in the π-back donation, become doubly occupied because the number of d electrons increases. Thereby, each of π_x^* and π_y^* orbitals has almost one electron. As a result, the electron populations of the π* orbitals of ethylene and dinitrogen significantly increase when going from Cr to Mn. However,

they change little when going from Mn to Ni, because some of singly-occupied non-bonding d MOs become doubly occupied when going from Mn to Ni.

The spin distribution is much interesting, too. In both of the ethylene and dinitrogen ISTCs of Sc to Cr, the spin population on the sandwiched ligand is negligibly small even in the high spin state. In the dinitrogen ISTCs of Mn to Ni, on the other hand, a significantly large negative spin population is found on the dinitrogen ligand, while it is nearly zero in their ethylene analogues; see Table S5. We will discuss the reason of this difference in the next section.

3.4. Difference and similarity between ethylene and dinitrogen ISTCs of M = Mn to Ni.

The reason of all the differences shown in Table S5 will be discussed below based on some of important orbitals.

3.4.1. Distorted geometry of the ethylene moiety and non-distorted one of the dinitrogen moiety in Mn to Ni complexes. The distorted C_{2h} symmetry of the ethylene ISTCs of Mn to Ni arises from the presence of the singly occupied $\psi_{11,ag}$ MO, as was discussed above. In the η^1-end-on dinitrogen ISTCs of Mn to Ni, on the other hand, the anti-bonding $\psi_{12,b2g}$ is unoccupied in a formal sense, as shown in Figure 4(B); note that the moderate occupation number (about 0.6 e) of the $\psi_{12,b2g}$ arises from one- and two-electron excitations from the $\psi_{1,b2g}$ to the $\psi_{12,b2g}$. This electron configuration arises from the presences of one more bonding $\psi_{2,b3g}$ MO and one more anti-bonding $\psi_{11,b3g}$ MO in the dinitrogen ISTCs; remember that two π_x^* and π_y^* orbitals of the dinitrogen ligand interact with the d_{xz} and d_{yz} orbitals of two metal centers to form two sets of bonding and anti-bonding MOs in the η^1-end-on complex. The other reason is the difference in π^* orbital energy between dinitrogen and ethylene. Because the dinitrogen molecule has a triple bond, the π^* orbital exists at a higher energy than that of ethylene. As a result, the

$\psi_{11,b3g}$ and $\psi_{12,b2g}$ of the η^1-end-on dinitrogen ISTCs mainly consisting of the π^* orbitals of dinitrogen exist at a higher energy than the $\psi_{11,ag}$ of the ethylene ISTCs: see Table S7 in SI. Because of these situations, one more electron can occupy not the $\psi_{11,b3g}$ but the $\psi_{2,b3g}$ when going from Cr to Mn in the case of the η^1-end-on dinitrogen ISTCs; see Figure 4(B). Thus, the $\psi_{11,b3g}$ MO does not become singly occupied in the dinitrogen ISTC of Mn.

In the Fe analogue, two more electrons occupy the $\psi_{3,b1u}$ and $\psi_{4,ag}$ because the anti-bonding $\psi_{11,b3g}$ and $\psi_{12,b2g}$ MOs are at high energy. In the Co complex, two more electrons occupy $\psi_{5,au}$ and $\psi_{6,b1g}$. In the Ni complex, two more electrons occupy $\psi_{7,b1u}$ and $\psi_{8,ag}$. In all these complexes, the anti-bonding $\psi_{11,b3g}$ and $\psi_{12,b2g}$ are empty in a formal sense. Because the $\psi_{11,b3g}$ and $\psi_{12,b2g}$ are unoccupied, there is no reason for the geometry distortion in these dinitrogen ISTCs.

3.4.2. Spin multiplicity and spin population on the bridging ligand. It is of considerable interest to elucidate the reason why the ground state of the dinitrogen ISTCs has an open-shell singlet spin multiplicity for M = Sc to Cr but a high spin multiplicity for M = Mn to Ni, as discussed above; see also Tables 2 and S5. In the dinitrogen ISTCs of Mn to Ni which have a singly occupied non-bonding ψ_{10} MO, the second and third leading configurations of the CASSCF wavefunction contain one-electron excitations from the doubly occupied $\psi_{1,b2g}$ and $\psi_{2,b3g}$ to the empty $\psi_{11,b3g}$ and $\psi_{12,b2g}$; see Table S8 in SI. These excitations increase ß-spin density on the dinitrogen π_x^* and π_y^* orbitals and the α-spin one on the d_{xz} and d_{yz} orbitals.[42] Because two α-spin electrons occupy $\psi_{9,b2u}$ and $\psi_{10,b3u}$ MOs mainly consisting of the metal d_{xz} and d_{yz} in these complexes, the above-mentioned excitations increase the exchange interaction on the metal centers; in other words, the presence of the singly occupied $\psi_{9,b2u}$ and $\psi_{10,b3u}$ induces the one-electron excitation from the $\psi_{1,b2g}$ and $\psi_{2,b3g}$ to the $\psi_{11,b3g}$ and $\psi_{12,b2g}$ so as to increase the α-spin

population on the metal centers and enlarge the exchange interaction.[43]

In the dinitrogen ISTCs of Sc to Cr, on the other hand, the above-mentioned one-electron excitation does not necessarily occur because the non-bonding $\psi_{10,b3u}$ (d_{yz}) MO is unoccupied due to the smaller number of d electrons. Hence, the spin polarization is not induced and the negative spin population does not appear on the dinitrogen ligand. Because of the absence of spin polarization, the high spin state does not receive additional stabilization from the exchange interaction. This is one reason why the ground state does not have high spin multiplicity.

Interestingly, the negative spin population on the dinitrogen ligand decreases as going from Mn to Ni. This result is understood with the number of singly occupied non-bonding d MOs. The number of singly occupied MOs decreases but that of doubly occupied MOs increases as going from Mn to Ni, because the number of d electrons increases. These singly occupied MOs mainly consisting of non-bonding d orbital contribute to the spin polarization. Hence, the extent of spin polarization decreases as going from Mn to Ni, leading to the decrease in negative spin population on the dinitrogen ligand. This is also the reason why the dinitrogen ISTCs of Mn to Ni have a high spin ground state; remember that the exchange interaction is enhanced by spin polarization in these complexes.

In contrast to the dinitrogen ISTCs of Mn to Ni, no spin population is found on the π^* orbital of ethylene in all ethylene ISTCs even at a high spin state; see Tables 5 and S5. In the ethylene ISTCs of Sc to Cr, the $\psi_{10,b3u}$ MO mainly consisting of the d_{yz} is empty in a formal sense. In this electronic structure, one-electron excitation from the $\psi_{1,b2g}$ to the anti-bonding $\psi_{11,b2g}$ does not enhance the exchange interaction with the $\psi_{10,b3u}$. In other words, the spin polarization does not occur and thereby the high spin state is not stabilized well. In the ethylene ISTC of Mn, the $\psi_{1,b2g}$ MO mainly consisting of the π^* orbital of ethylene is doubly occupied and all other non-bonding and anti-bonding d MOs

are singly occupied. Thus, the excited configuration from the $\psi_{1,b2g}$ to the anti-bonding $\psi_{11,b2g}$ MO does not increase the number of singly occupied MO not to contribute to the increase in α-spin population on the metal d-orbital; in other words, the spin polarization does not occur, too, leading to the absence of negative spin population on the ethylene moiety.

In the ethylene ISTCs of Mn to Ni, not a high spin state but an open-shell singlet is the ground state, despite that ten to four MOs consisting of d orbital are singly occupied in these Mn to Ni complexes. Such orbital occupation suggests that these complexes would have a high spin ground state. However, we must remember that the M-M distance is considerably long in these ethylene ISTCs because the ethylene coordinates with two metal centers in μ-η^1:η^1-mode in which the ethylene carbons have an sp^3-like structure; see Figure 2. In this structure, it is likely that the exchange interaction between two distant metal centers is very small and thereby there is no reason that the high spin state is the ground state. Moreover, the spin-polarization does not occur; see above. As a result, the open-shell singlet becomes the ground state, while the energy difference between the open-shell singlet and the high spin state is very small.

3.4.3. The evidence of the important role of a singly occupied non-bonding d orbital. In the above section, we discussed that the non-bonding MOs mainly consisting of d_{yz} and d_{xz} play crucial roles in inducing spin polarization and thereby providing a high spin ground state. However, no evidence was presented. To provide a theoretical evidence of the above discussion, we carried out several model calculations. If the above explanation is correct, the ground state of the ethylene ISTC of Cr must have a high spin multiplicity by adding one electron to the non-bonding $\psi_{10,b3u}$. Also, the ground state of the ethylene ISTC of Mn must have a high spin multiplicity by removing one electron from the $\psi_{11,b2g}$ because one-electron excitation from the $\psi_{1,b2g}$ to the $\psi_{11,b2g}$ can occur in such electronic

state. The various spin states of such mono-anionic (μ-C_2H_4)[Cr(AIP)]$_2^-$ and mono-cationic (μ-C_2H_4)[Mn(AIP)]$_2^+$ were calculated by the CASPT2 method, where their geometries were taken to be the same as those of the neutral Cr and Mn analogues under D_{2h} symmetry because we want here to focus on the difference in electronic structure. As shown in Table 6, the dectet spin state is the ground state in both of Cr and Mn complexes; see Table S9 for occupation numbers of CASSCF natural orbitals. The important difference from the neutral analogue is that the occupation number of the anti-bonding $\psi_{11,b2g}$ MO remarkably increases but that of the $\psi_{1,b2g}$ decreases. This is because the singly occupied non-bonding $\psi_{10,b3u}$ MO induces the spin polarization by the one-electron excitation from the $\psi_{1,b2g}$ to the $\psi_{11,b2g}$. Also, it is noted that the large negative spin population is found on the π* orbital of ethylene like the dinitrogen ISTCs of Mn to Ni; see Table 6. Based on these results, it is concluded that the singly occupied non-bonding d MO and the unoccupied anti-bonding MO play crucial roles for presenting a high spin ground state and a negative spin population on the bridging ligand.

4. Conclusions

We theoretically investigated the inverse sandwich-type dinuclear complexes, (μ-C_2H_4)[M(AIP)]$_2$ and (μ-N_2)[M(AIP)]$_2$, for 3d transition metals from Sc to Ni. The geometry and the electronic structure are similar between the ethylene and dinitrogen ISTCs of Sc to Cr because the dinitrogen molecule has the η^2-side-on coordination which is essentially the same as the ethylene coordination structure. In the ethylene and η^2-side-on dinitrogen complexes, the very stable bonding $\psi_{1,b2g}$ MO is formed by the bonding overlap between the d_{yz} orbitals of two metal atoms and the π* orbital of the bridging ethylene and η^2-side-on dinitrogen molecules. This MO is doubly occupied in a formal sense. Other MOs mainly consisting of d orbital are singly occupied. This electronic structure is essentially the same between the ethylene and the η^2-side-on dinitrogen

complexes. Both of the ethylene and the η^2-side-on dinitrogen complexes have an open-shell singlet ground state because some of non-bonding MOs can have a larger occupation number than their anti-bonding counterparts and the spin-polarization does not occur due to the absence of singly occupied non-bonding d_{yz} MO.

In Mn to Ni, on the other hand, the bonding nature and the spin multiplicity are completely different between the ethylene and dinitrogen ISTCs. In the ethylene ISTCs of Mn to Ni, each carbon atom of ethylene coordinates with one metal atom in a μ-η^1:η^1-coordination mode. In these complexes, the strongly anti-bonding ψ_{11} MO becomes singly occupied in the D_{2h} geometry, because of the larger number of d electrons than in M = Sc to Cr. As a result, the distortion to a C_{2h} geometry occurs to reduce the anti-bonding overlap of the $\psi_{11,ag}$ MO between the d_{yz} orbitals of metals and the π^* orbital of ethylene. In the C_{2h} geometry, the d orbital component considerably increases and the π^* component of the ethylene moiety considerably decreases in the $\psi_{11,ag}$ MO, which leads to the increase of the π^* component in the $\psi_{1,ag}$ MO. Hence, the hybridization of ethylene carbon changes from sp^2 to sp^3. This means that the ethylene moiety becomes di-anion-like, in which each carbon atom has one sp^3-lone pair orbital and it coordinates with one metal atom. Though the ground state of these complexes is singlet, the energy difference among spin states is very small.

In the dinitrogen ISTC of Mn, the η^1-end-on and η^2-side-on dinitrogen coordination structures are comparable in energy. In the ISTCs of Sc to Cr, the η^2-side-on structure is considerably more stable than the η^1-end-on one. This is because one very stable d_{yz}-π_z^* MO is doubly occupied in the η^2-side-on dinitrogen ISTCs of Sc to Cr but two considerably stable d_{yz}-π_y^* and d_{xz}-π_x^* MOs are doubly occupied in the η^1-end-on dinitrogen ISTC of Mn. However, the η^1-end-on structure becomes more stable than the η^2-side-on one as going from Mn to Ni because the d orbital energy becomes lower and the σ-donation to metal 3d, 4s, and 4p from the lone pair of dinitrogen becomes stronger

in the η^1-end-on structure; note the π orbital of dinitrogen is less favorable for the σ-donation than the lone pair orbital. In these η^1-end-on dinitrogen ISTCs of Mn to Ni, the high spin state is much more stable than the singlet state because the spin polarization occurs to enhance the exchange interaction with the non-bonding d MO; remember that the non-bonding d MO is singly occupied in these complexes and the one-electron excitation is possible from the stable bonding MO to the empty anti-bonding MO.

In our study, it is clearly shown that some of non-bonding and/or weakly anti-bonding MOs play crucial roles for determining geometry and spin multiplicity of these complexes. We wish to emphasize that one can control the magnetism of this ISTC by either adding one electron to or removing one electron from the crucial non-bonding MO.

ACKNOWLEDGEMENTS

This work is financially supported by Grant-in-Aids of Specially Promoted Science and Technology (No. 22000009) and Grants-in-Aids for Scientific Research (No. 15H03770) from Ministry of Education, Culture, Sports, Science, and Technology. SS is thankful for Japan Science and Technology Cooperation (CREST 'Establishment of Molecular Technology towards the Creation of New Functions' Area). We are also thankful to the computational facility at the Institute of Molecular Science, Okazaki, Japan.

NOTES AND REFERENCES

Fukui Institute for Fundamental Chemistry, Kyoto University, Takano-Nishihiraki-cho, Sakyo-ku, Kyoto 606-8103, Japan E-mail: sakaki.shigeyoshi.47e@st.kyoto-u.ac.jp

† Electronic Supplementary Information (ESI) avairable: Relative energies of η^1-end and η^2-side structures calculated by CASPT2 method with two different active spaces (Table S1); Rerative energies of spin state including spin-orbit coupling (Table S2); Geometrical parameters of ethylene ISTC of Cr (Table S3); Effective magnetic moment ethylene ISTC

of Cr with various structures (Table S4); Potential energies of ethylene ISTC of Cr along ethylene rotation (Figure S1); Similarities and differences between ethylene and dinitrogen ISTCs (Table S5); MO diagram of M(AIP) (Figure S2); MO diagram of benzene ISTC of Cr (Figure S3); Schematic pictures of d orbital energy splitting (Figure S4); Relative energies of spin states at CASSCF level (Table S6); Bonding MO of dinitrogen ISTC of Cr with η^2-side-on and η^1-end-on structures (Figure S5); CASSCF orbitals of $(\mu\text{-}\eta^2\text{:}\eta^2\text{-}N_2)[Mn(AIP)]_2$ (Figure S6); Orbital energies of C_2H_4 and N_2 (Table S7); Main configurations of CASSCF and CASCI wavefunction (Table S8); Occupation numbers of CASSCF orbitals in $[(\mu\text{-}\eta^2\text{:}\eta^2\text{-}C_2H_4)[Cr(AIP)]_2]^-$ and $[(\mu\text{-}\eta^2\text{:}\eta^2\text{-}C_2H_4)[Mn(AIP)]_2]^+$ (Table S9).

1 M. Mannini, F. Pineider, C. Danieli, F. Totti, L. Sorace, Ph. Sainctavit, M.-A. Arrio, E. Otero, L. Joly, J. C. Cezar, A. Cornia, R. Sessoli, *Nature*, 2010, **468**, 417.

2 K. Goss, D. Gatteschi, L. Bogani, *Phys. Chem. Chem. Phys.*, 2014, **16**, 18076.

3 D. N. Woodruff, R. E. P. Winpenny, R. A. Layfield, *Chem. Rev.*, 2013, **113**, 5110.

4 A. Bousseksou, G. Molnar, L. Salmon, W. Nicolazzi, *Chem. Soc. Rev.*, 2011, **40**, 3313.

5 M. A. Halcrow, *Chem. Soc. Rev.*, 2011, **40**, 4119.

6 K. P. Kepp, *Coord. Chem. Rev.*, 2013, **257**, 196.

7 L. Triguero, L. G. M. Pettersson, *J. Chem. Phys.* 1998, **108**,1993.

8. B. Minaev, H. Ågren , *J. Mol. Catal. A: Chem.*, 1999, **149**, 179.

9. S. V. Bondarchuk, B. F. Minaev, *Chem. Phys.Lett.*, 2014, **607** 75.

10. S. V. Bondarchuk, B. F. Minaev, *RSC Adv.*, 2015, **5**, 11558.

11 V. C. Gibson, C. Newton, C. Redshaw, G. A. Solan, A. J. P. White, D. J. Williams, *Eur. J. Inorg. Chem.*, 2001, 1895.

12 G. Bai, P. Wei, D. M. Stephan, *Organometallics*, 2005, **24**, 5901.

13 J. M. Smith, A. R. Sadique, T. R. Cundari, K. R. Rodgers, G. L.- Rodgers, R. J. Lachicotte, C. J. Flaschenriem, J. Vela, P. L. Holland, *J. Am. Chem. Soc.*, 2006, **128**, 756.

14 W. H. Monillas, G. P. A. Yap, L. A. MacAdams, K. H. Theopold, *J. Am. Chem. Soc.*, 2007, **129**, 8090.

15 W. H. Monillas, G. P. A. Yap, K. H. Theopold, *Angew. Chem.,Int. Ed.*, 2007, **46**, 6692.

16 Y.-C. Tsai, P.-Y. Wang, S.-A. Chen, J.-M. Chen, *J. Am. Chem. Soc.*, 2007, **129**, 8066.

17 Y.-C. Tsai, P.-Y. Wang, K.-M. Lin, S.-A. Chen, J.-M. Chen, *Chem. Commun.*, 2008, 205.

18 S. Pfirrmann, C. Limberg, C. Herwig, R. Stößer, B. Ziemer, *Angew. Chem.*, 2009, **121**, 3407.

19 S. Pfirrmann, S. Yao, B. Ziemer, R. Stösser, M. Driess, C. Limberg, *Organometallics*, 2009, **28**, 6855.

20 P. L. Holland, *Dalton Trans.*, 2010, **39**, 5415.

21 P. L. Diaconescu, C. C. Cummins, *Inorg. Chem.*, 2012, **51**, 2902.

22 T. L. Gianetti, G. Nocton, S. G. Minasian, N. C. Tomson, A. L. D. Kilcoyne, S. A. Kozimor, D. K. Shuh, T. Tyliszczak, R. G. Bergman, J. Arnold, *J. Am. Chem. Soc.*, 2013, **135**, 3224.

23 T. Jurca, I. Korobkov, S. I. Gorelsky, D. S. Richeson *Inorg. Chem.*, 2013, **52**, 5749.

24 F. Aguilera-Granja, R. H. Aguilera-del-Toro, A.Vega, L. C. Balbás, *J. Phys. Chem. A*, 2014, **118**, 2976.

25. T. L. Gianetti, G. Nocton, S. G. Minasian, N. Kaltsoyannis, A. L. D. Kilcoyne, S. A. Kozimor, D. K. Shuh, T. Tyliszczak, R. G. Bergman, J. Arnold, *Chem. Sci.*, 2015, **6**, 993.

26 Y. I. Kurokawa, Y. Nakao, S. Sakaki, *J. Phys. Chem. A*, 2010, **114**, 1191.

27 Y. I. Kurokawa, Y. Nakao, S. Sakaki, *J. Phys. Chem. A*, 2012, **116**, 2292.

28 M. Nakagaki, S. Sakaki, *J. Phys. Chem. A*, 2014, **118**, 1247.

29 B. O. Roos, *Adv. Chem. Phys.*, 1987, **69**, 399.

30 K. Andersson, P.- Å. Malmqvist, B. O. Roos, A. J. Sadlej, K. Wolinski, *J. Phys. Chem.*, 1990, **94**, 5483.

31 K. Andersson, P.- Å. Malmqvist, B. O. Roos, *J. Chem. Phys.*, 1992, **96**, 1218.

32 B. O. Roos, K. Andersson, *Chem. Phys. Lett.*, 1995, **245**, 215.

33 C. Edmiston, K. Ruedenberg, *Rev. Mod. Phys.*, 1963, **35**, 457.

34 M. Dolg, U. Wedig, H. Stoll, H. Preuss, *J. Chem. Phys.*, 1987, **86**, 866.

35 T. H. Dunning, Jr., *J. Chem. Phys.*, 1989, **90**, 1007.

36 M. W. Schmidt, K. K. Baldridge, J. A. Boatz, S. T. Elbert, M. S. Gordon, J. J. Jensen, S. Koseki, N. Matsunaga, K. A. Nguyen, S. Su, T. L. Windus, M. Dupuis and J. A. Montgomery, *J. Comput. Chem.*, 1993, **14**, 1347.

37 G. Karlström, R. Lindh, P.-Å. Malmqvist, B. O. Roos, U. Ryde, V. Veryazov, P.-O. Widmark, M. Cossi, B. Schimmelpfennig, P. Neogrady, L. Seijo, *Comput. Mater. Sci.*, 2003, **28**, 222.

38 Because it is very difficult to optimize the geometry on the two-dimensional potential energy surface by CASPT2 calculation, we optimized first the Cr-Cr distance in the D_{2h} geometry and then optimized the deviation between two Cr-C distances by increasing one Cr-C distance and simultaneously decreasing another Cr-C distance by 0.015Å. The Cr-Cr distance was optimized to be 4.055 Å, as shown in Figure S1(A), and the deviation between two Cr-C distances monotonously induces energy destabilization, as shown in Figure S1(B). These results indicate that the D_{2h} symmetry is more stable than the C_{2h} one.

39 (a) This result indicates that the CASPT2 method overestimates the stability of low spin state. However, the effective magnetic moment is sensitive to the energy gap among

these spin states. If the singlet and the triplet states become unstable by 1.2 kcal/mol and the septet and the nonet states become stable by 1.2 kcal/mol, the magnetic moment is estimated to be 3.6 μ_B, which is close to the experimental value. Considering the size of active space, the geometry of model, the neglect of solid phase effect, and the complicated electronic structure of (μ-C_2H_4)[M(AIP)]$_2$, an error of 1 - 2 kcal/mol is not very large.

(b) Another plausible origin of the too small effective magnetic moment would be the difference between the optimized and experimental geometries. However, the CASPT2 calculation with the experimental geometry provided an effective magnetic moment of 1.5 μ_B, which is almost the same as the value calculated with the optimized geometry; see Table S4 in SI.

40 Because the doubly occupied C-C and N-N σ-bonding MOs much less contribute to these MOs than the metal d orbital, it is not easy to show both of the σ-bonding MOs and the metal d orbital in the same figure. These σ-bonding MOs are shown in larger size in Figure S4.

41 The $\psi_{1,b2g}$ and $\psi_{2,b3g}$ MOs are doubly occupied in a formal sense though the occupation numbers of them are about 1.46 and 1.43, as shown in Figure 4(B) and Table 4. Several excited configurations from the $\psi_{1,b2g}$ and $\psi_{2,b3g}$ to the $\psi_{11,b3g}$ and $\psi_{12,b2g}$ considerably contribute to the wavefunction.

42 The sixth and seventh configurations consist of one-electron excitation of α-spin from the ψ_1 and ψ_2 to the ψ_{11} and ψ_{12}, the CI expansion coefficients of which are reverse to those of the third and the second terms; see Table S8. As a result, α-spin population increases on metal d orbitals and ß-one increases on ethylene in all these excited configurations.

43 The $\psi_{1,b2g}$ and $\psi_{12,b2g}$ consist of d_{yz} and π_y* orbitals and the $\psi_{2,b3g}$ and $\psi_{11,b3g}$ consist of d_{xz} and π_x* orbitals in the η^1-end-on, as shown in Figure 4(B). Because the $\psi_{10,b3u}$ and $\psi_{9,b2u}$ have the same d orbital compounds as the ψ_1/ψ_{12} and ψ_2/ψ_{11}, respectively, the

exchange interaction by these orbitals are large.

Table 1. Relative energies (in kcal/mol) of various spin multiplicities in (μ-C_2H_4)[M(AIP)]$_2$ (M = Sc to Ni) with various spin multiplicities calculated by the CASPT2 method under D_{2h} and C_{2h} symmetries.

spin	Sc		Ti		V		Cr	
multiplicity	C_{2h}	D_{2h}	C_{2h}	D_{2h}	C_{2h}	D_{2h}	C_{2h}	D_{2h}
9							5.5	5.8
7					2.2	2.7	4.1	3.8
5			12.4	1.2	1.4	1.5	2.8	2.0
3	7.4	0.3	11.9	0.5	0.7	0.6	1.8	0.8
1	7.3	0.0	11.6	0.0	0.3	0.0	1.2	0.0
spin	Mn		Fe		Co		Ni	
multiplicity	C_{2h}	D_{2h}	C_{2h}	D_{2h}	C_{2h}	D_{2h}	C_{2h}	D_{2h}
11	1.8	29.4						
9	1.4	28.4	1.2	24.1				
7	1.0	26.8	0.9	21.2	0.8	15.6		
5	0.6	25.6	0.6	18.1	0.6	11.1	0.1	21.3
3	0.3	24.7	0.3	16.3	0.3	7.7	0.1	11.1
1	0.0	24.1	0.0	15.1	0.0	5.8	0.0	6.9

Table 2. Relative energies (in kcal/mol) of (μ-N_2)[M(AIP)]$_2$ (M = Sc to Ni) with various spin multiplicities calculated by the CASPT2 method.

spin	Sc		Ti		V		Cr	
multiplicity	η^2-side	η^1-end	η^2-side	η^1-end	η^2-side	η^1-end	η^2-side	η^1-end
9							3.1	24.6
7					1.4	35.2	2.1	19.9
5			1.7	20.8	0.9	21.4	1.2	15.3
3	0.4	21.6	0.8	19.9	0.4	17.5	0.4	12.2
1	0.0	19.3	0.0	18.1	0.0	15.9	0.0	10.5
spin	Mn		Fe		Co		Ni[a)]	
multiplicity	η^2-side	η^1-end	η^2-side	η^1-end	η^2-side	η^1-end	η^2-side	η^1-end
9	0.0	0.2						
7	5.0	5.2	3.9	0.0				
5	9.4	9.6	10.0	7.3	4.8	0.0		
3	13.9	13.9	15.9	14.2	13.9	11.3	15.1	0.0
1	18.7	18.4	22.3	21.9	24.3	24.4	47.8	30.5

a) In the Ni complex, occupied π orbitals of dinitrogen are involved in active space. See also Table S1 in SI.

Table 3. Occupation numbers of the CASSCF natural orbitals in (μ-C_2H_4)[M(AIP)]$_2$ (M = Sc to Ni) in the open-shell singlet ground state.

	(μ-η^2:η^2-C_2H_4)[M(AIP)]$_2$					(μ-η^1:η^1-C_2H_4)[M(AIP)]$_2$				
MO	main component	Sc	Ti	V	Cr	main component	Mn	Fe	Co	Ni
ψ_{11}	φ_5^a–π^*	0.01	0.01	0.01	0.01	φ_5^a	1.01	0.98	1.08	1.09
ψ_{10}	φ_5^b	0.02	0.03	0.04	0.05	φ_5^b	0.99	1.02	1.08	1.09
ψ_9	φ_4^b				0.97	φ_4^b	1.00	1.00	1.92	1.09
ψ_8	φ_4^a				1.03	φ_4^a	1.00	1.00	1.92	1.09
ψ_7	φ_3^b			0.96	0.98	φ_3^b	1.00	1.00	1.06	2.00
ψ_6	φ_3^a			1.04	1.02	φ_3^a	1.00	1.00	1.06	2.00
ψ_5	φ_2^b		0.97	0.98	0.99	φ_2^b	1.00	1.00	1.92	1.91
ψ_4	φ_2^a		1.03	1.02	1.01	φ_2^a	1.00	1.00	1.92	1.91
ψ_3	φ_1^b	1.05	0.96	0.99	1.00	φ_1^b	1.00	2.00	1.00	1.91
ψ_2	φ_1^a	0.95	1.04	1.01	1.00	φ_1^a	1.00	2.00	1.00	1.91
ψ_1	φ_5^a+π^*	1.97	1.97	1.96	1.94	π^*	2.00	2.00	2.00	2.00

Table 4. Occupation numbers of CASSCF natural orbitals in (μ-N_2)[M(AIP)]$_2$ (M = Sc to Ni).

MO	(μ-η^2:η^2-N_2)[M(AIP)]$_2$					(μ-η^1:η^1-N_2)[M(AIP)]$_2$				
	main component	Sc	Ti	V	Cr	main component	Mn	Fe	Co	Ni
		1et	1et	1et	1et		9et	7et	5et	3et
ψ_{12}	$\varphi_5^a-\pi_z^*$	0.00	0.02	0.03	0.01	$\varphi_5^a-\pi_y^*$	0.54	0.50	0.49	0.43
ψ_{11}	π^*_x	0.01	0.03	0.04	0.01	$\varphi_4^a-\pi_x^*$	0.57	0.55	0.51	0.45
ψ_{10}	φ_5^b	0.01	0.03	0.05	0.02	φ_5^b	1.00	1.00	1.00	1.00
ψ_9	φ_4^b			0.02	0.94	φ_4^b	1.00	1.00	1.00	1.01
ψ_8	φ_4^a			0.02	1.06	φ_3^b	1.00	1.00	2.00	2.00
ψ_7	φ_3^b			1.00	1.01	φ_3^a	1.00	1.00	2.00	2.00
ψ_6	φ_3^a			0.98	0.99	φ_2^b	1.00	1.00	1.00	2.00
ψ_5	φ_2^a		0.87	0.90	0.97	φ_2^a	1.00	1.00	1.00	2.00
ψ_4	φ_2^b		1.10	1.04	1.02	φ_1^b	1.00	2.00	2.00	2.00
ψ_3	φ_1^b	1.08	1.02	1.01	1.00	φ_1^a	1.00	2.00	2.00	2.00
ψ_2	φ_1^a	0.92	0.98	0.98	1.00	$\varphi_4^a+\pi_x^*$	1.43	1.45	1.48	1.55
ψ_1	$\varphi_5^a+\pi_z^*$	1.97	1.95	1.95	1.96	$\varphi_5^a+\pi_y^*$	1.46	1.50	1.52	1.58

Table 5. Electron and spin populations on the π* orbitals of N_2 and C_2H_4 moieties in (μ-N_2)[M(AIP)]$_2$ and (μ-C_2H_4)[M(AIP)]$_2$ (M = Sc to Ni) calculated by the CASCI method with the localized molecular orbitals.

	(μ-N_2)[M(AIP)]$_2$							
	Sc	Ti[a)]	V[a)]	Cr	Mn	Fe	Co	Ni
	3et	5et	7et	9et	9et	7et	5et	3et
Electron								
$\pi_{z/y}$*	1.11	1.14	1.27	1.27	0.98	0.94	0.96	0.96
π_x*	0.01			0.08	0.97	0.96	0.94	0.91
total	1.12	1.14	1.27	1.35	1.95	1.90	1.90	1.87
Spin								
$\pi_{z/y}$*	−0.01	−0.03	−0.05	−0.09	−0.69	−0.62	−0.54	−0.38
π_x*	0.00			0.08	−0.71	−0.64	−0.56	−0.37
total	−0.01	−0.03	−0.05	0.00	−1.40	−1.26	−1.10	−0.76
	(μ-C_2H_4)[M(AIP)]$_2$							
	Sc	Ti	V	Cr	Mn	Fe	Co	Ni
	3et	5et	7et	9et	11et	9et	7et	5et
Electron	0.98	1.00	1.11	1.13	2.00	2.00	2.00	2.00
Spin	−0.01	−0.03	−0.03	−0.05	0.00	0.00	0.00	0.00

a) In the Ti and V complexes, the N_2 π_x* MO was excluded from active space in this analysis because the N_2 π_x* MO mix to metal $4d_{xy}$ orbitals.

Table 6. Relative energies (in kcal/mol) of various spin multiplicities of $[(\mu\text{-}\eta^2\text{:}\eta^2\text{-}C_2H_4)[Cr(AIP)]_2]^-$ and $[(\mu\text{-}\eta^2\text{:}\eta^2\text{-}C_2H_4)[Mn(AIP)]_2]^+$ and electron and spin populations on the π* orbital of the C_2H_4 moiety at the dectet spin state.

Spin multiplicity	$[(\mu\text{-}\eta^2\text{:}\eta^2\text{-}C_2H_4)[Cr(AIP)]_2]^-$	$[(\mu\text{-}\eta^2\text{:}\eta^2\text{-}C_2H_4)[Mn(AIP)]_2]^+$
	Relative energy	
12	79.5	40.0
10	0.0	0.0
8	2.3	2.8
6	4.6	5.6
4	7.3	8.5
2	10.5	11.6
	Electron and spin populations on π* of C_2H_4[a)]	
Electron population	1.31	1.04
Spin population	−0.40	−0.68

a) In the dectet spin state. These values are evaluated from occupation numbers of the localized orbital.

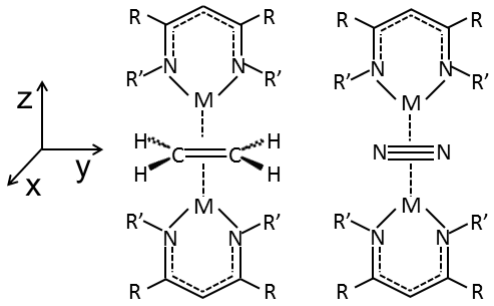

Figure 1. (μ-C_2H_4)[M(N^N)]$_2$ and (μ-N_2)[M(N^N)]$_2$ (M = Sc-Ni; N^N = DDP (DDPH = 2-{(2,6-diisopropylphenyl)amino}-4-{(2,6-diisopropylphenyl)imino}pent-2-ene) or AIP (AIPH = (Z)-1-amino-3- imino-prop-1-ene)). R = Me, R' = 2,6-$^{i}Pr_2C_6H_3$ in DDP and R = R' = H in AIP.

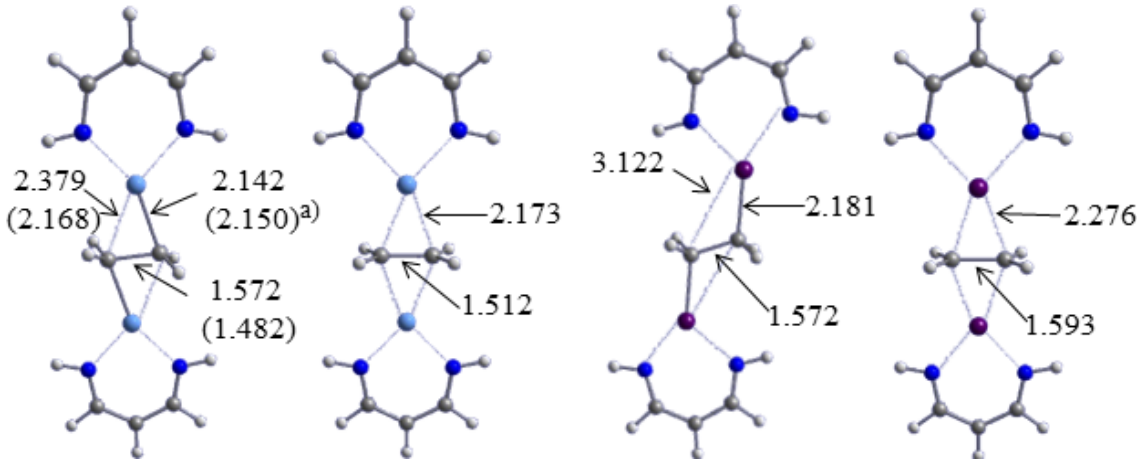

C_{2h} D_{2h} C_{2h} D_{2h}

R(Cr-Cr)= 4.246 Å R(Cr-Cr)= 4.074 Å R(Mn-Mn)= 5.151 Å R(Mn-Mn)= 4.264 Å

(R(Cr-Cr) exp. = 4.057 Å)[b)]

(A) (μ-C_2H_4)[Cr(AIP)]$_2$ **(B) (μ-C_2H_4)[Mn(AIP)]$_2$**

Figure 2. Optimized structures of (μ-C_2H_4)[M(AIP)]$_2$ (M = Cr, Mn) calculated by the CASSCF method under C_{2h} and D_{2h} symmetries with an open-shell singlet state.

a) Parentheses are experimental values.

b) The experimental value of (μ-C_2H_4)[Cr(DDP)]$_2$.

(A) (μ-η²:η²-C₂H₄)[Cr(AIP)]₂

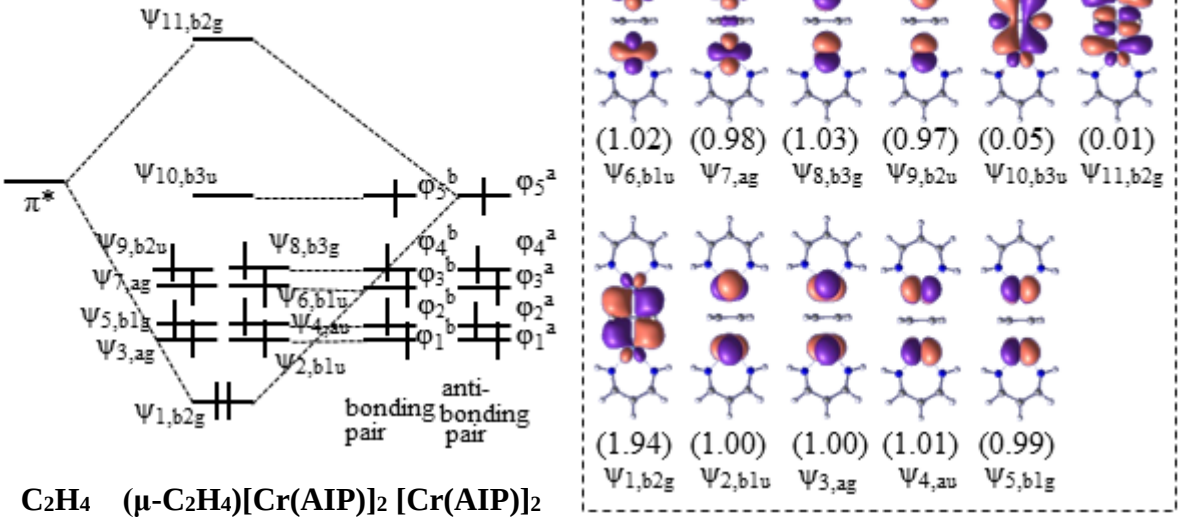

C₂H₄ (μ-C₂H₄)[Cr(AIP)]₂ [Cr(AIP)]₂

(B) (μ-η¹:η¹-C₂H₄)[Mn(AIP)]₂

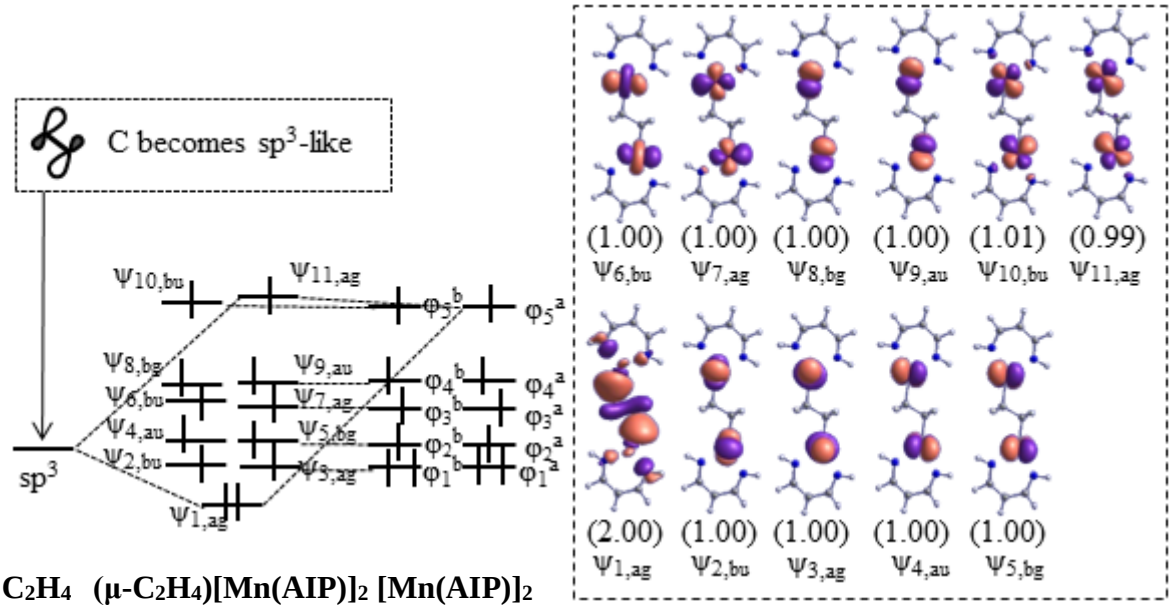

C₂H₄ (μ-C₂H₄)[Mn(AIP)]₂ [Mn(AIP)]₂

Figure 3. Schematical orbital interaction diagrams of (A) (μ-η²:η²-C₂H₄)[Cr(AIP)]₂ and (B) (μ-η¹:η¹-C₂H₄)[Mn(AIP)]₂. In dashed line are natural orbitals with occupation numbers.

(A) (μ-η²:η²-N₂)[Cr(AIP)]₂

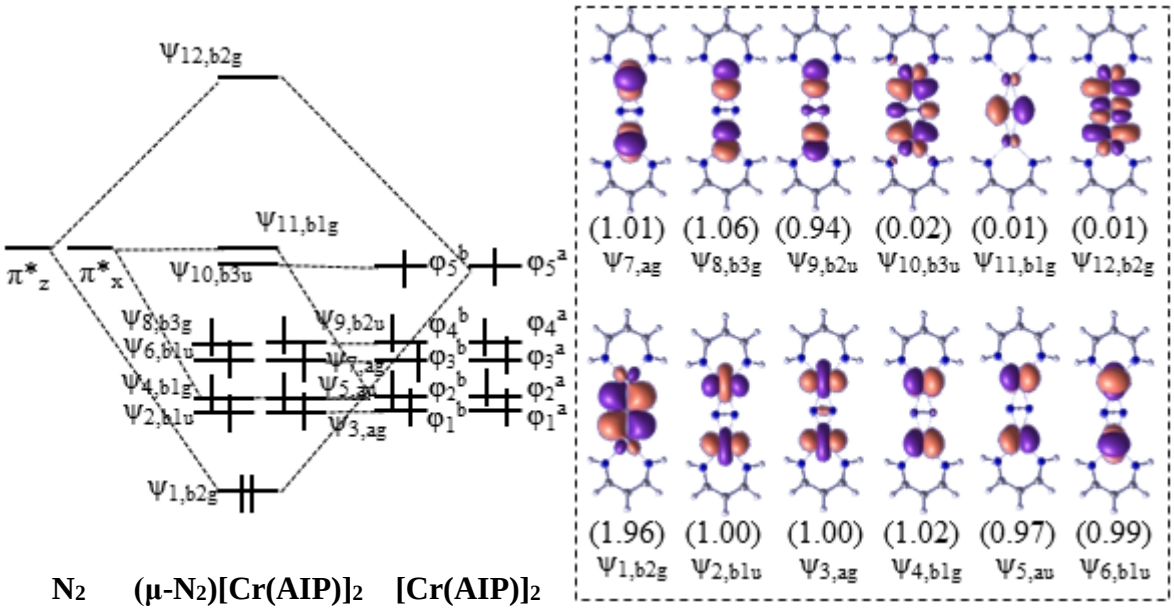

N₂ (μ-N₂)[Cr(AIP)]₂ [Cr(AIP)]₂

(B) (μ-η¹:η¹-N₂)[Mn(AIP)]₂

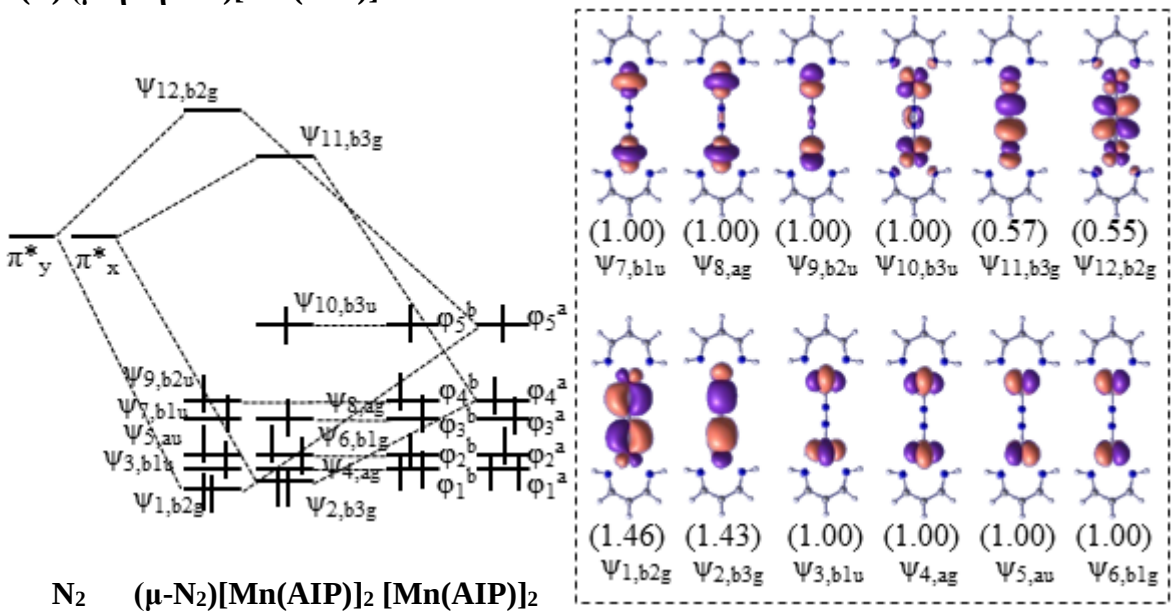

N₂ (μ-N₂)[Mn(AIP)]₂ [Mn(AIP)]₂

Figure 4. Schematical orbital interaction diagrams of (A) (μ-η²:η²-N₂)[Cr(AIP)]₂ and (B) (μ-η¹:η¹-N₂)[Mn(AIP)]₂. In dashed line are natural orbitals with occupation numbers.

Table of Content (Graphics)